A COMPARISON OF SKYLAB S-193 AND AIRCRAFT VIEWS OF SURFACE ROUGHNESS AND A LOOK TOWARD SEASAT

M-2

By Duncan Ross, Sea-Air Interaction Laboratory, National Oceanic and Atmospheric Administration, Atlantic Oceanographic and Meteorological Laboratories, Miami, Florida

ABSTRACT

An extensive aircraft underflight program was conducted along the Skylab groundpath for the purpose of documenting wind, wave, and atmospheric conditions affecting the amplitude of the active and passive microwave signatures. The S-193 microwave system senses a roughness parameter at the ocean surface that is proportional to the surface windspeed. The exact relationship between the wind and this roughness parameter is the subject of continuing investigations.

In the case of the active portion of the system, the intensity of off-nadir backscatter from the ocean is thought to be primarily determined by the amplitude of short gravity/capillary waves and has been shown to be strongly a function of azimuth relative to the surface wind direction. The passive side of the instrument senses the naturally emitted (and reflected) microwave energy and is proportional to the RMS slope and percent foam coverage of the ocean.

NOAA, NASA, and USAF aircraft were equipped with a variety of environmental sensors in an attempt to specify the surface conditions affecting the satellite sensors as well as active and passive microwave sensors intended to calibrate the Skylab instrument. The aircraft program is described, and some comparisons of satellite and aircraft results are presented. The principal result of the comparison of active radar is that direct inferences of the surface windspeed are possible, but subject to considerable scatter, and that this scatter appears to be due to interaction between long gravity and short Bragg waves and backscatter due to rain as well as errors in correcting for azimuth dependence. It is shown that σ_0 for incidence angles of $\approx 50°$ increases both with windspeed and with increasing energy level of the high-frequency gravity waves that, themselves, are proportional to both the local wind and fetch in a manner that is not uniquely determined by the windspeed.

An unforeseen opportunity to observe a Pacific hurricane by both Skylab and NOAA aircraft has contributed to the development of a simplified wave forecasting scheme applicable to hurricanes, and more general conditions, which combines the better qualities of both spectral and height/period forecasting techniques. The implication of this result to the SEASAT program is that quite large data inputs in both the time and space domain can be handled using existing computers and should produce a forecast of comparable or superior quality to existing spectral techniques, but in shorter time steps. Horizontal polarization data obtained by the aircraft in Hurricane Ava, and in other experiments, which led to this development are presented.

INTRODUCTION

The S-193 experiment aboard Skylab was intended to test the concept of remote determination of surface wind conditions on a worldwide basis as an aid to improved environmental forecasts. A part of this experiment included an aircraft underflight program to calibrate and validate the inference of surface wind conditions from the satellite measurements of radar backscatter, σ_0, and upwelling naturally emitted microwave energy, T_a.

A number of significant developments have evolved as a result of this combination of satellite and aircraft studies of the environment, which will be touched upon herein. It is impossible, however, to discuss in depth all aspects included in the scope of this program. Results presented here are preliminary, and some conclusions may be modified as additional data sets are considered. The reader is, therefore, asked to be tolerant of missing details and tentative conclusions that, hopefully, will be firmed up in future reports.

AIRCRAFT INSTRUMENTATION

The aircraft measurements were obtained from instrumented NOAA, NASA, and USAF C130 aircraft. All aircraft were equipped with a basic environmental package consisting of an inertial platform for windspeed determination, a Barnes Infrared Radiometer for sea surface temperatures, a laser wave profiler for wave measurements, a Cambridge Dew Point Hygrometer, a Rosemount Air Temperature Probe, and a vertical camera for white-cap photography. The NOAA C130 was additionally equipped with a three-frequency passive microwave system at K_u (14.5 GHz), X (8.35 GHz), and L (1.8 GHz) bands. This system was used for dual polarization measurements at X and K_u bands and horizontal polarization measurements at L-band. Because the NOAA aircraft was not available for the third launch period, a cooperative arrangement with the Air Force 53rd Weather Reconnaissance Squadron of the Air Weather Service was negotiated by NOAA, and the inertial platform, laser, microwave, and camera systems were transferred to the Air Force C130 for the SL-4 underflight program. Figure 1 shows the NOAA C130 aircraft with passive microwave antennas extended to the in-flight operating position.

The NASA JSC C130 aircraft was similarly equipped except that the microwave system was both active and passive (time-shared) and centered only at 13.5 GHz. The NASA aircraft participated in the underflight program during all three launch periods.

SATELLITE INSTRUMENTATION

Skylab S-193 Instrument. The S-193 experiment aboard Skylab consists of an instrument capable of operation in one of three modes: (1) short pulse altimetry, (2) radar backscatter, and (3) a passive radiometer mode. The instrument is a single-frequency device centered at 13 GHz (K_u band). In the so-called RADSCAT configuration, the instrument alternately switches between the active and passive mode. It is capable of scanning in the along-track and across-track directions, and thus obtains dual polarization measurements of radar backscattering cross section, σ_0, and

upwelling naturally emitted microwave energy, which is directly proportional to the apparent, or antenna, temperature T_a, as a function of incidence angle.

Radar Backscatter. The mechanisms responsible for determining the level of radar energy backscattered by the ocean surface are primarily, but not limited to, the amplitude of resonant Bragg waves for incidence angles between about 30° and 80°, and the RMS slope distribution for near vertical incidence angles (Wright, 1968; Valenzuela, 1968). The Bragg condition is defined as

$$\frac{2\pi}{\lambda_{water}} = K_B = K_0 \cos \theta_1 + K_0 \cos \theta_2$$

where θ_1 and θ_2 are the incident and scattering angles, $K_0 = 2\pi/\lambda$ microwave. In the case of S-193, these waves correspond to cm wavelength ocean waves. The detailed behavior of Bragg waves and also their effect on backscatter has been the subject of considerable study in laboratory experiments in recent years (cf. Rouse and Moore, 1972; Duncan, Keller, and Wright, 1974; Keller, Larson, and Wright,1974; Keller and Wright, 1975; Reece and Shemdin, 1974; and many others). The principal result of these studies is that the backscattered doppler radar spectrum for a particular radar frequency and incidence angle is not a unique function of windspeed but rather is, to some degree, a function of fetch, duration, and presence of swell as well as windspeed.

The Wave Spectrum. It has been suggested that the S-193 RADSCAT data are affected by both long and short ocean waves. In the following sections, an attempt will be made to evaluate S-193 data in terms of the wave spectrum. A brief description of the spectrum and its behavior during growth and swell situations is therefore appropriate.

Wave conditions can be fully described by the two-dimensional energy spectrum, $A^2(f,\theta)$, and integration over direction (θ) and frequency, f, yields the total energy

$$E = \int_0^\infty \int_{-\pi}^{\pi} [A(f,\theta)]^2 \, d\theta df$$

which is proportional to mean surface displacement, $2\sigma^2$.

For a wind blowing off a shoreline, the fetch is defined simply as the distance from shore to the downwind measurement site. Figure 2 presents the behavior of the one-dimensional energy spectrum for seven fetch locations during offshore wind conditions as observed in the JONSWAP experiment (Hasselmann et. al., 1973). The inset of Figure 2 depicts the meaning of the five parameters suggested by Hasselmann et. al. as convenient for describing the important characteristics of the spectrum. It can be seen from this figure that the peak frequency, f_m, grows and migrates toward lower frequencies as fetch increases. Hasselman et. al. found that the sharpness parameter, γ, and the width parameters σ_a, σ_b, are essentially independent of fetch. The Phillips parameter, α, however, generally decreased with increasing fetch. The behavior of the spectral scale parameters can also be represented

conveniently in nondimensional form by incorporation of the local windspeed, U_{10}, and gravity. Thus, Figure 3 presents the behavior of nondimensional energy

$$\tilde{E} = \frac{Eg^2}{U_{10}{}^4}$$

and nondimensional frequency

$$\tilde{f}_m = \frac{f_m U_{10}}{g}$$

versus nondimensional fetch

$$\tilde{X} = \frac{xg}{U_{10}{}^2}.$$

Nondimensionalization in this manner has properly accounted for the windspeed dependence of the behavior of total energy and peak frequency with fetch. The interrelationship between α, $\tilde{E}$, and $\tilde{f}_m$ is therefore apparent and was studied in detail by Hasselmann et. al. (1975). They proposed $\tilde{f}_m$ as a convenient means of describing the stage of development of the wave spectrum in an average sense. Figures 4 and 5 from this study show the behavior of $\tilde{E}$ and α with respect to $\tilde{f}_m$ and $\tilde{X}$. The lines denoted

$$C_\omega = 10^{-3}$$

and

$$C_\omega = 10^{-5}$$

are representative of the momentum entering the wave field (Hasselmann et. al., 1973), with an approximate mean value of

$$C_\omega \approx 10^{-4},$$

or about 20 percent of the total momentum transferred to the ocean by the wind. Variations about the mean are attributed to changes in the local wind conditions. An example of varying the wind by a factor of 1.5 for a particular f_m is included in the figures.

RESULTS

Because the principal purpose of the S-193 experiment was to remotely infer surface wind conditions, it is appropriate to first consider examples of the data from a typical pass as a prelude to more extensive analysis of the complete data set. Figure 6 presents the results of a pass in the Gulf of Mexico during SL-2 and is a typical example of variable low windspeed conditions. The S-193 active radar backscattering cross sections, (σ_0), and passive microwave antenna temperature, T_a, for horizontal polarization and an incidence angle of 50° are shown plotted as a function of latitude along with the surface wind conditions as determined from the NOAA aircraft underflight.

Considerable variability can be seen for σ_0, especially around 19° and 22° N. The data for those latitudes less than 23°, however, were not corrected for azimuth dependence and therefore show scatter due to changes in wind direction as well as speed. The higher latitudes, however, are of most interest because they were accompanied by extensive ground truth. It can be seen that the surface winds decreased significantly between 24° and 26° N, while σ_0 decreased only slightly between 24° and 25.5° N and actually increased at 26° N. The horizontally polarized antenna temperature agrees well with aircraft determinations and also increases significantly at 26° N. Because of the presence of many rain showers observed by the aircraft to be in the area of 26° N, these increases are tentatively attributed to this factor. This pass, therefore, implies significant corrections would normally be required to account for the presence of rain.

During SL-2, a unique opportunity to observe high wind conditions developed with the appearance of a hurricane in the eastern Pacific southwest of Acapulco, Mexico (Ross et. al., 1974). As plans were being formulated for observing the storm with the S-193 system, the NOAA C130 aircraft deployed on the 6th of June to Acapulco, refueled, and flew a 7.5-hour mission into the storm. Figure 7 is a NOAA-2 composite satellite view of Hurricane Ava showing the flight track of Skylab as it conducted a data pass with S-193 operating in the side-looking solar inertial mode. Unfortunately, the storm was rapidly moving away from the subsatellite track and it was not possible to obtain measurements in the region of maximum winds. Figure 8 is an example of active and passive measurements of Ava obtained at incidence angles of 42.5° and 50.5° along with estimates of surface winds obtained during the aircraft penetration and rainfall rates estimated from the NIMBUS-5 satellite 19.35 passive microwave system (Wilheit, 1972). It can be seen from this figure that there is an increase in σ_0 and T_a in the higher wind areas of the storm with the highest antenna temperature occurring in the zone of heavy rainfall.

High wind conditions were also obtained during the third launch period. Figure 9 shows the subsatellite track for data obtained on the 9th of January at incidence angles of 0° and $\pm \approx 50°$ along with the NOAA surface analysis for 1800Z. This situation is particularly interesting because the windspeed varied from 7.5 to 30 m/sec from the beginning to the end of the sampling period with little rainfall reported except in the region of the front. Figure 10 presents the variation in σ_0 and T_a for +47.6° and -50.5° incidence angle along with surface winds estimated from an isotach analysis based mainly on ship reports and the NASA JSC aircraft measurements. A qualitative comparison of these data sets, together with that from Hurricane Ava and the June 11 pass in the Gulf of Mexico, strongly suggests a first-order dependency on surface wind conditions but with scatter.

Unfortunately, due to damage to the S-193 antenna occurring during an SL-3 extravehicular excursion, the antenna pattern was altered in an unknown fashion. It is therefore risky to include the 9 January data set with those obtained during SL-2 when calculating windspeed dependency. This case was therefore treated separately and is shown plotted against windspeed in Figure 11. σ_0 and T_a data obtained during SL-2 are shown in Figure 12 plotted against windspeed. These data sets are restricted to those data passes described above, which were accompanied by an aircraft underflight. Aircraft-determined antenna temperatures included show good agreement with S-193. The surface winds attached to each satellite data point are judged to be accurate to about 1 to 3 m/sec in the case of SL-2 and 3 to 5 m/sec in the case of the SL-4 pass of 9 January. The judgment of accuracy includes the effects of mesoscale variability in the local wind conditions and inaccuracies associated with aircraft-determined winds and ship reports in the case of

the 9 January data. Unfortunately, no study is known to the author that compares ship reports (mostly visual estimates) to continuously recorded and calibrated winds averaged over 10 to 30 minutes. Therefore, one is left with a judgment.

DISCUSSION

The above data sets strongly suggest a useful first-order relationship between surface winds for both σ_0 and T_a subject to some degree of scatter. There are several sources of errors in both parameters contributing to the scatter that crops up in the processing. In addition, there may be errors due to invalid atmospheric assumptions (or errors in the corrections required for a particular assumption), random errors in inferring the 10-meter windspeed from aircraft measurements, as well as natural variability in local wind conditions. The above errors inherent to this data set probably cannot be reduced any further.

One potential source of error that can be addressed, however, lies in the lack of uniqueness of the active or passive signature due to the variability in possible wave conditions that may be present for a given windspeed. Reece and Shemdin (1974), in a study conducted in a wave tank, showed that the high-frequency waves, for a particular fetch, are windspeed dependent, but the absolute energy level for a particular windspeed is reduced with the addition of a low-frequency component (swell) and that the amount of the reduction is proportional to the amplitude of the low-frequency component. Mitsuyasu (1971) showed similar reduction in the high-frequency gravity region of the wave spectrum with the introduction of swell. Hasselmann et. al. (1973), showed that the Phillips constant (α) (Phillips, 1958), which determines the energy level of the f^{-5} region of the wave spectrum, decreases with increasing nondimensional fetch as discussed earlier. In order to assess the possible importance of the gravity wave spectrum in this data set, it is desirable to consider σ_0 as a function of some observable parameter of the wave field that varies with fetch in a well-behaved and predictable manner.

The nondimensional peak frequency, $\tilde{f}_m$, was shown earlier to be a particularly useful parameter that well describes the stage of development of the wave spectrum. Aircraft measurements of the wave spectrum were used directly to specify f_m for Skylab data sets obtained on 5 and 11 June 1973. The data for Hurricane Ava, however, present a special problem because the aircraft measurements were not obtained at the exact subsatellite point. In order to specify the peak frequency, it was desirable to develop some technique of estimating these parameters from the aircraft data set. The hurricane wind fields are circular in nature, however, and the fetch relationship needed to infer $\tilde{f}_m$ is ambiguous and arbitrary. Furthermore, the position of the aircraft measurements relative to the eye of the hurricane were concentrated in the rear quadrant, whereas most of the satellite positions were to the right of the hurricane center. Figure 13, however, presents some of the wave data obtained, plotted along with spectra from the North Sea measured under similar wind conditions, but fetch limited, and in the North Atlantic during fully developed conditions. The resemblance between the spectra is striking. The most significant feature of the Ava spectra, however, is the general lack of "swell," which would appear as a secondary peak in the spectrum. This is especially significant when the unidirectional assumption required in processing the aircraft data is considered. Because we assume all waves are moving in a direction parallel to the aircraft flight track, swell from some other direction is moved toward lower frequencies in the mapping process to fixed coordinates, leading to an unrealistic "broad"

appearance to the spectrum with multiple peaks. Hurricane Ava was a superhurricane by any criteria and had a record low pressure for eastern Pacific storms of 914 millibars. Fortunately, another such storm of which wave measurements have recently become available was Hurricane Camille, one of the worst hurricanes to ever strike the coast of the United States as it went ashore near Mobile, Alabama, in August of 1969. Camille's eye dimensions, maximum winds, forward velocity, and central pressure were virtually identical to those of Hurricane Ava. Measurements of wave conditions in relatively deep water were obtained by a consortium of oil companies. Some of the data were reported recently (Patterson, 1974, and Hamilton and Ward, 1974) and were used in this study. Figure 14 presents the relative positions of Camille and Ava wave data to the eye and wind field of Ava as determined from the NOAA aircraft flight. It is fortunate that Camille was so similar to Ava as the windspeeds measured on the oil company platform were biased low because of poor anemometer exposure for a storm approaching in the direction of Camille. Ava's winds were therefore used to specify the Camille wind field, which avoids the difficulty of introducing another empirically based technique to specify 10-meter anemometer winds. The wave data from Camille and Ava were then nondimensionalized and plotted against the nondimensional radial distance from the eye and are presented in Figure 15. It can be seen that a simple power law reasonably well describes the radial behavior of both $\tilde{E}$ and $\tilde{f}_m$. Nondimensional peak frequencies for the Ava data set were therefore calculated from the expression.

$$\tilde{f}_m = 1.6\tilde{R}^{-.25}$$

where

$$\tilde{R} = \frac{rg}{U_{10}{}^2}$$

and r is the particular radial distance from the subsatellite point to the eye of Ava. The Ava data set was then combined with data from 5 and 11 June 1973 and is shown in Figure 16. It can be seen that σ_0 varies considerably with $\tilde{f}_m$. It can be argued that, because the windspeed is included in the calculation of $\tilde{f}_m$, it is difficult to correctly separate the windspeed dependency from stage of development. To aid in this separation of dependencies, a multiple regression analysis was performed according to the equation

$$Z = a_0 + a_1x + a_2y$$

letting $Z = \sigma_0$, $x = U_{10}$, and $y = \tilde{f}_m$. The constants a_0, a_1, and a_2 were found to be -29.5, 0.20, and 59.4, respectively. Such a dependency on $\tilde{f}_m$ is much greater than expected or would be predicted on the basis of wave tank experiments cited earlier. The same multiple regression analysis was performed on the 9 January data set, based on hindcast $\tilde{f}_m$, for 47.6° incidence angle, and yielded values of -15.7, 0.39, and 17.5 for the same constants. The hindcast performed assumed limited fetch, but unlimited duration, and the rather low wave heights reported suggest an underestimate for the values of $\tilde{f}_m$ for the higher winds. Also possible is a bias in the case of the hurricane data set due to backscatter from rain. The 9 January data set, however, seems to confirm a fetch dependency and both sets considered together suggest that controlled high-wind, variable-fetch experiments should be performed to accurately infer high winds from measurements of σ_0.

A similar treatment of the fetch effect in the case of the passive microwave measurements is also indicated and is underway.

RELATION TO SEASAT

The success of the simplified approach suggested by Hasselmann et. al. (1975) for specifying the evolution of the wave spectrum depends on successful parameterization of the nonlinear interactions that control the exchange of energy within the spectrum that, in turn, are very sensitive to local gustiness in the surface wind conditions. However, because it is not necessary to deal with the entire directional spectrum for each grid point in a numerical forecast scheme, it will be possible to increase the density of grid points and decrease the time steps involved in forecasting waves. For example, a typical spectral model consisting of 17 frequencies and 15 directions for 512 grid points in the North Atlantic requires 130 000 storage locations, whereas the simplified approach, expanded to account for two swell systems, can increase the grid density to 5012 and require only 30 072 locations. Such a forecasting approach is needed for rapid assimilation of satellite data and will likely be in operation by the time the SEASAT satellite is launched. At this time, the First Global GARP Experiment will also be underway and provide a unique opportunity to test the SEASAT concept.

CONCLUSIONS

The Skylab S-193 experiment has proved that active and passive microwave sensors can be used to infer surface winds but are subject to scatter and a decreasing sensitivity with increasing windspeed in the case of the active radar, and bias due to rainfall with little sensitivity to lower windspeeds in the case of passive microwave signatures. These results, therefore, suggest that combined active and passive systems with a weighted averaging process (employing polarization dependencies) being used to infer the local wind might reduce some of the scatter due to random errors and should be tested with Skylab data. The results further suggest that a parameterization of the wave spectrum may be necessary in order to further reduce the scatter in σ_0. The Skylab data set contains most of the data needed to test these hypotheses and could lead to satellite determination of both the windspeed and surface wave spectrum by judicious use of active and multifrequency passive microwave systems.

ACKNOWLEDGMENTS

The author is grateful to the many people in the satellite and aircraft program which comprised the Skylab experiment. Special thanks are due the NOAA C130 crew for expertly conducting 500 foot flight tracks in one of the most severe hurricanes of record, and the NASA JSC and USAF air crews for low-level flights into severe winter storms (especially the Air Force loadmaster who finally closed a balky cargo door allowing a planned high-altitude pressurized return to shore during one occasion). Finally, the accuracy and extent of passive microwave data collected by the NOAA and USAF aircraft is due to the diligence and competence of the Naval Research Laboratory and is greatly appreciated.

REFERENCES

Barnett, T. P., and J. C. Wilkerson (1967), On the generation of ocean wind waves as inferred from airborne radar measurements of fetch-limited spectra. J. Mar. Res. 25, 292.

Duncan, J. R., W. C. Keller, and J. W. Wright (1974), Fetch and wind speed dependence of Doppler spectra. Radio Science 9, No. 10, 809-819.

Hamilton, R. C., and E. G. Ward (1974), Ocean data gathering program-quality and reduction of data. Offshore Technology Conference Proceedings, OTC 2108-A, 750-756.

Hasselmann, K., T. P. Barnett, E. Bouws, H. Carlson, D. E. Cartwright, K. Enke, J. A. Ewing, H. Gienapp, D. E. Hasselmann, P. Kruseman, A. Meerburg, P. Muller, D. J. Olbers, K. Richter, W. Sell, and H. Walden (1973), Measurements of wind-wave growth and swell decay during the Joint North Sea Wave Project (JONSWAP), Deutsche Hydrogr. Z., Suppl. A(8°), No. 12.

Hasselmann, K., D. B. Ross, P. Mueller, and W. Sell (1975), A Parametrical Wave Prediction Model, submitted to Journal of Physical Oceanography.

Keller, W. C., T. R. Larson, and J. W. Wright (1974), Mean speeds of wind waves at short fetch. Radio Science 9, No. 12, 1091-1100.

Keller, W. C., and J. W. Wright (1975), Microwave scattering and the straining of wind-generated waves. Radio Science 10, No. 2, 139-147.

Mitsuyasu, H. (1971), Observations of the wind and waves in Hakata Bay. Rep. Res. Inst. Appl. Mech., Kyushu University, 19:37-74.

Patterson, M. M. (1974), Oceanographic Data from Hurricane Camille. Offshore Technology Conference Proceedings, OTC 2109.

Phillips, O. M. (1958), The equilibrium range in the spectrum of wind generated waves. J. Fluid Mech. 4(4), 426-434.

Pierson, W. J., and L. Moskowitz (1964), A proposed spectral form for fully developed wind seas based on the similarity theory of S. A. Kitaigorodskii. J. Geophys. Res. 69, 5181-5190.

Reece, A. M., and O. H. Shemdin (1974), Modulation of capillary waves by long waves. Symposium on Ocean Wave Measurement and Analysis, Amer. Soc. Civil Eng., New Orleans, Louisiana.

Ross, D., B. Au, W. Brown, and J. McFadden (1974), A remote sensing study of Pacific Hurricane Ava. Ninth International Symposium on Remote Sensing of Environment Proceedings, 15-19 April, 163-180.

Ross, D., and V. Cardone (1974), Observations of oceanic whitecaps and their relation to remote measurements of surface wind speed. J. Geophys. Res. 79, No. 3, 444-452.

Rouse, J. W., and R. K. Moore (1972), Measured surface spectrum dependence of back-scattering from rough surface. IEEE Trans. Antennas Propagat., AP-20, 211-214.

Valenzuela, G. R. (1968), Scattering of electromagnetic waves from a tilted, slightly rough surface. Radio Science 3, 1057-1066.

Wilheit, T. (1972), Nimbus-5 Users Guide, NASA Goddard Space Flight Center, Washington, D.C.

Wright, J. W. (1968), A new model for sea clutter, IEEE Trans. Antennas Propagat., AP-16, 217-223.

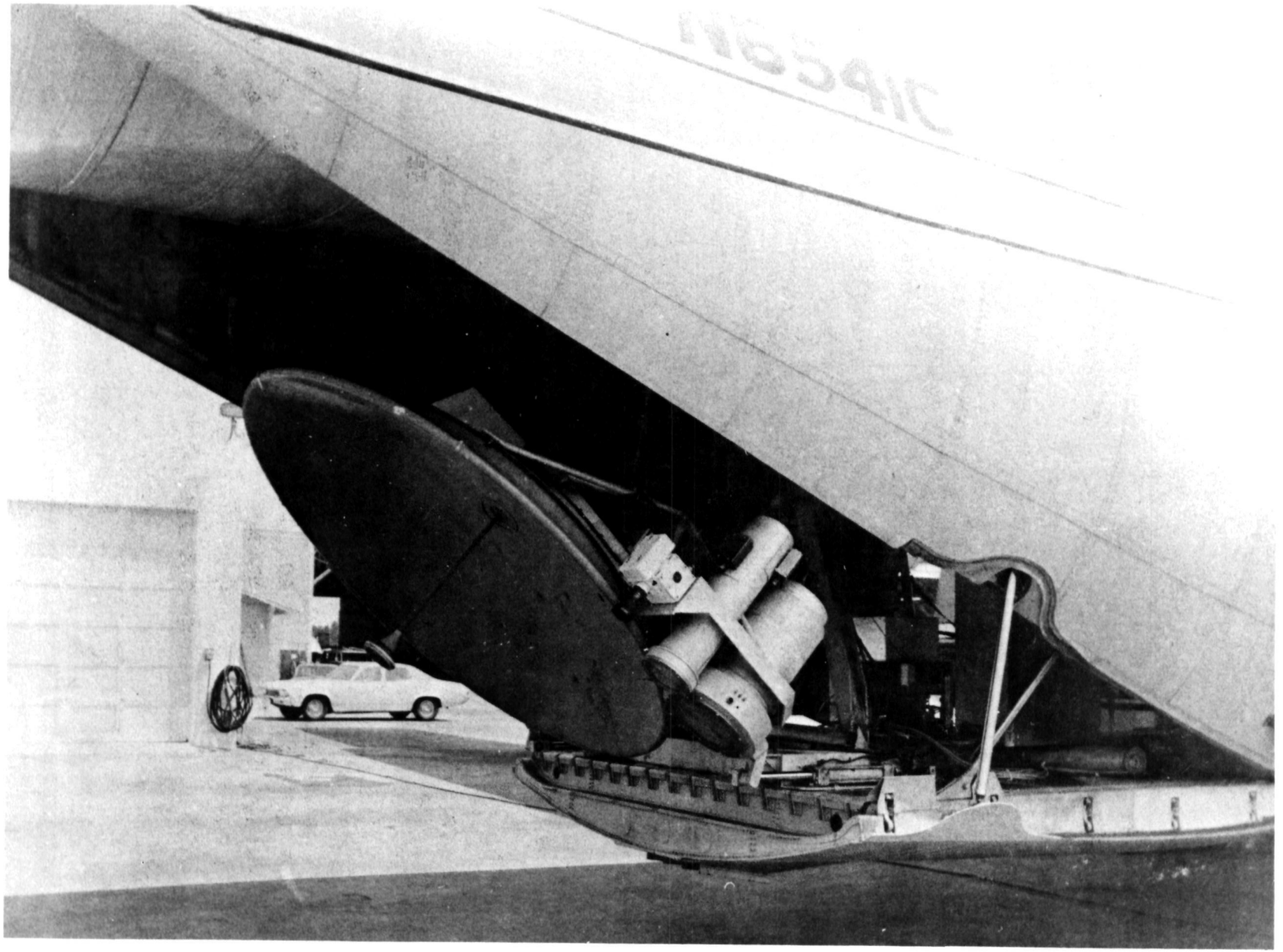

Figure 1. The NOAA C130 aircraft show passive microwave sensors in the extended position.

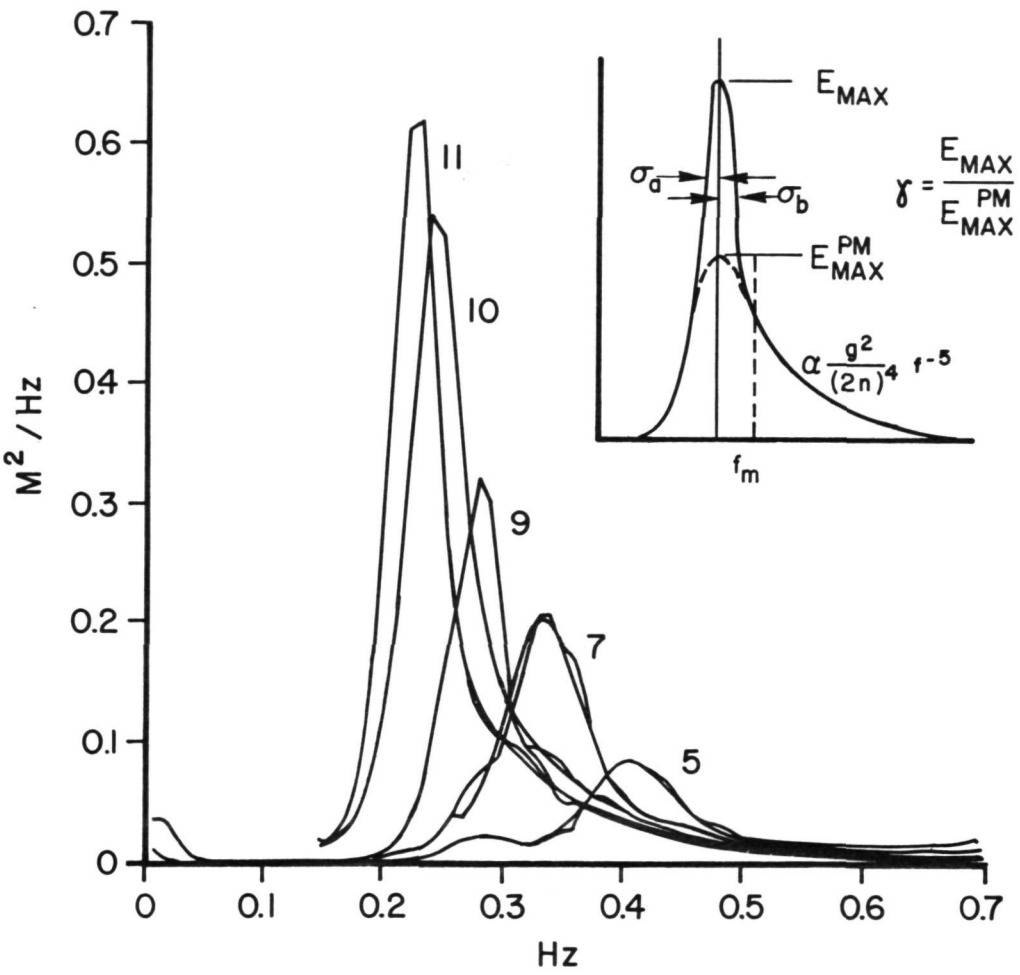

Figure 2. Growth of wave spectra for offshore wind conditions during JONSWAP-69. Fetch increases from Station 5 through Station 11. Three shape parameters σ_a, σ_b, and γ, and the scale parameters f_m and α suggested by Hasselmann are shown in the inset. γ is simply the ratio of the energy at f_m to that which would be predicted by the Pierson-Moskowitz (1964) form of the spectrum.

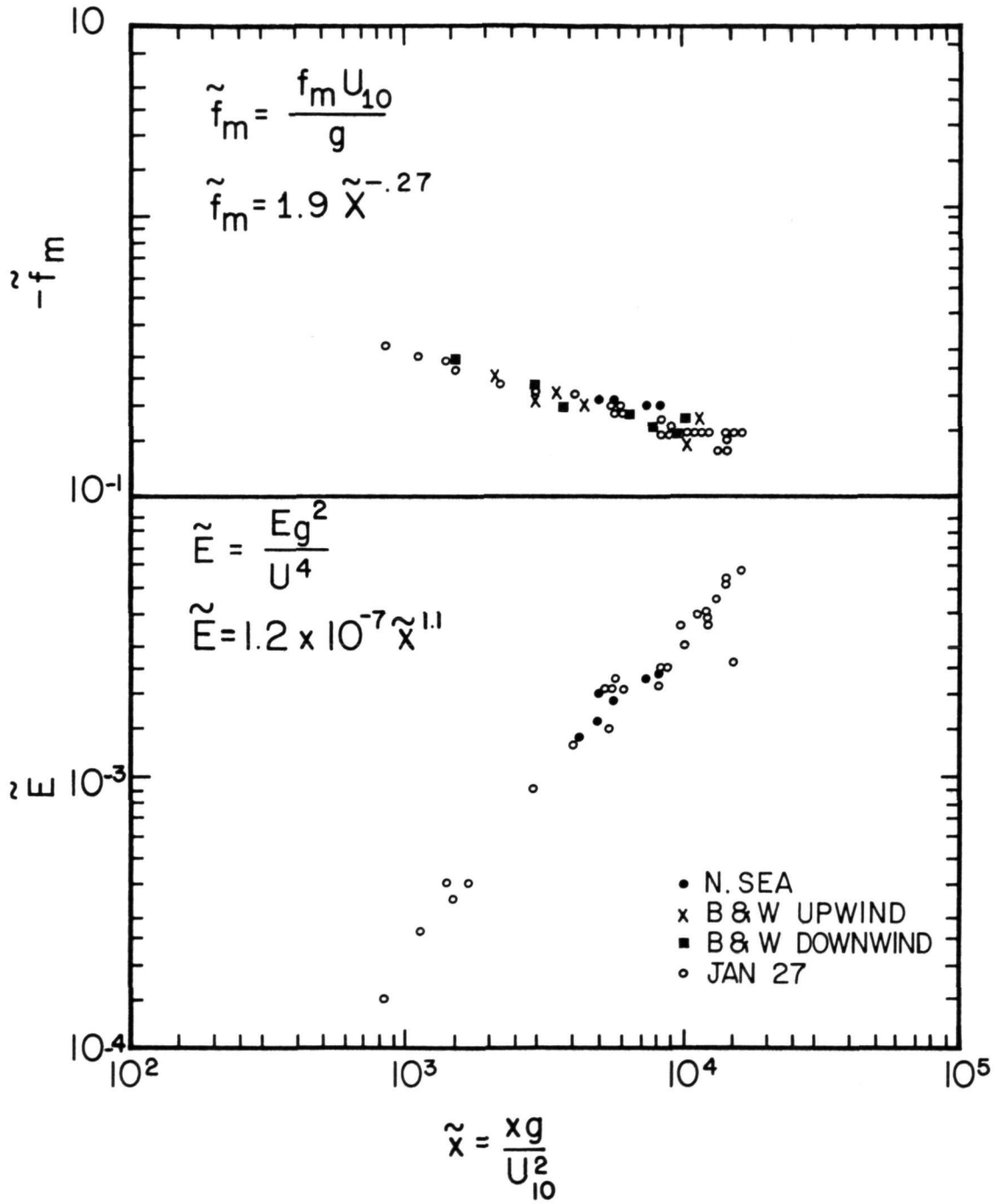

Figure 3. Dimensionless parameters $\tilde{E}$ and $\tilde{f}_m$ versus dimensionless fetch $\tilde{X}$ for high windspeeds (15 to 25 m/sec) as determined by aircraft experiments in the North Sea and off Cape Fear, N. C., on 27 January (Ross and Cardone, 1974, and Barnett and Wilkerson, 1969).

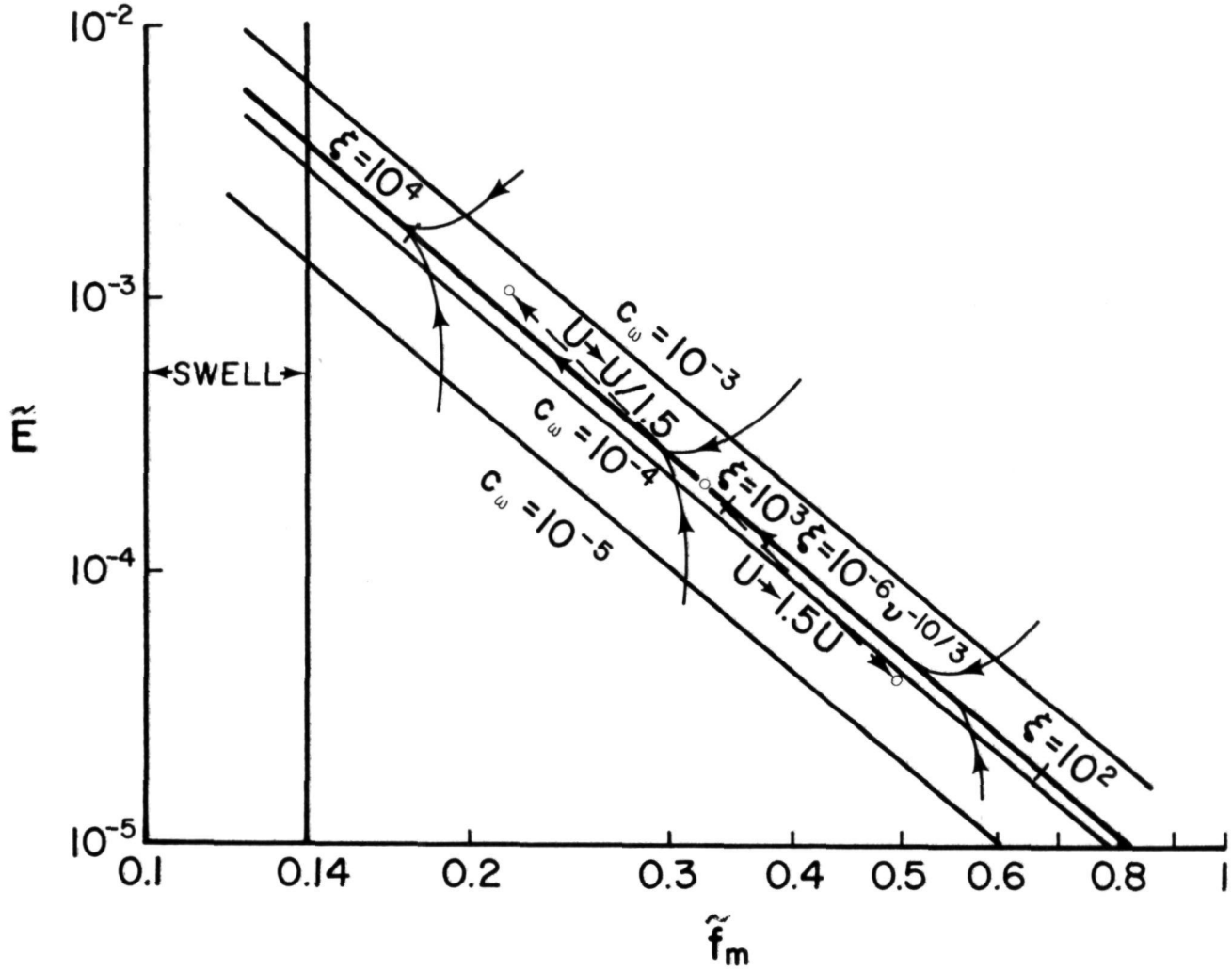

Figure 4. The behavior of $\tilde{E}$ and $\tilde{f}_m$ during growth. A sudden change of windspeed by a factor of 1.5 results in a departure from the mean followed by readjustment to mean condition along the curved lines indicated. Nondimensional fetch relationships $\tilde{X} = E = \frac{xg}{U_{10}{}^2}$ for particular $\tilde{f}_m$ are included. The upper and lower boundaries ($C_\omega = 10^{-3}$ and $C_\omega = 10^{-5}$) represent the limits of momentum being transferred to the wave spectrum.

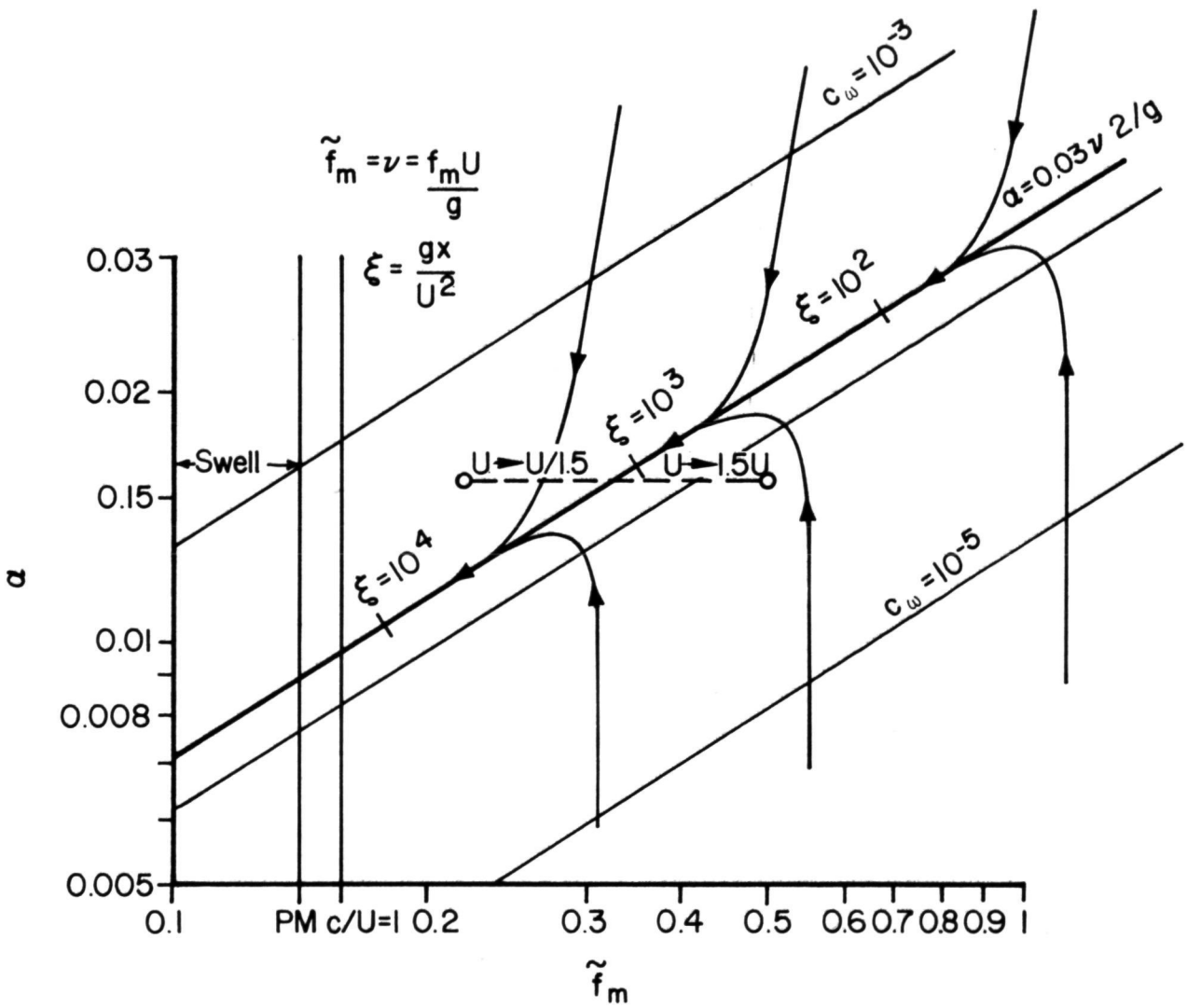

Figure 5. The Phillips parameter α versus $\tilde{f}_m$. Corresponding fetches ξ are indicated by the tick marks. The behavior of α during readjustment to a change in local wind (U) conditions is along the curved lines.

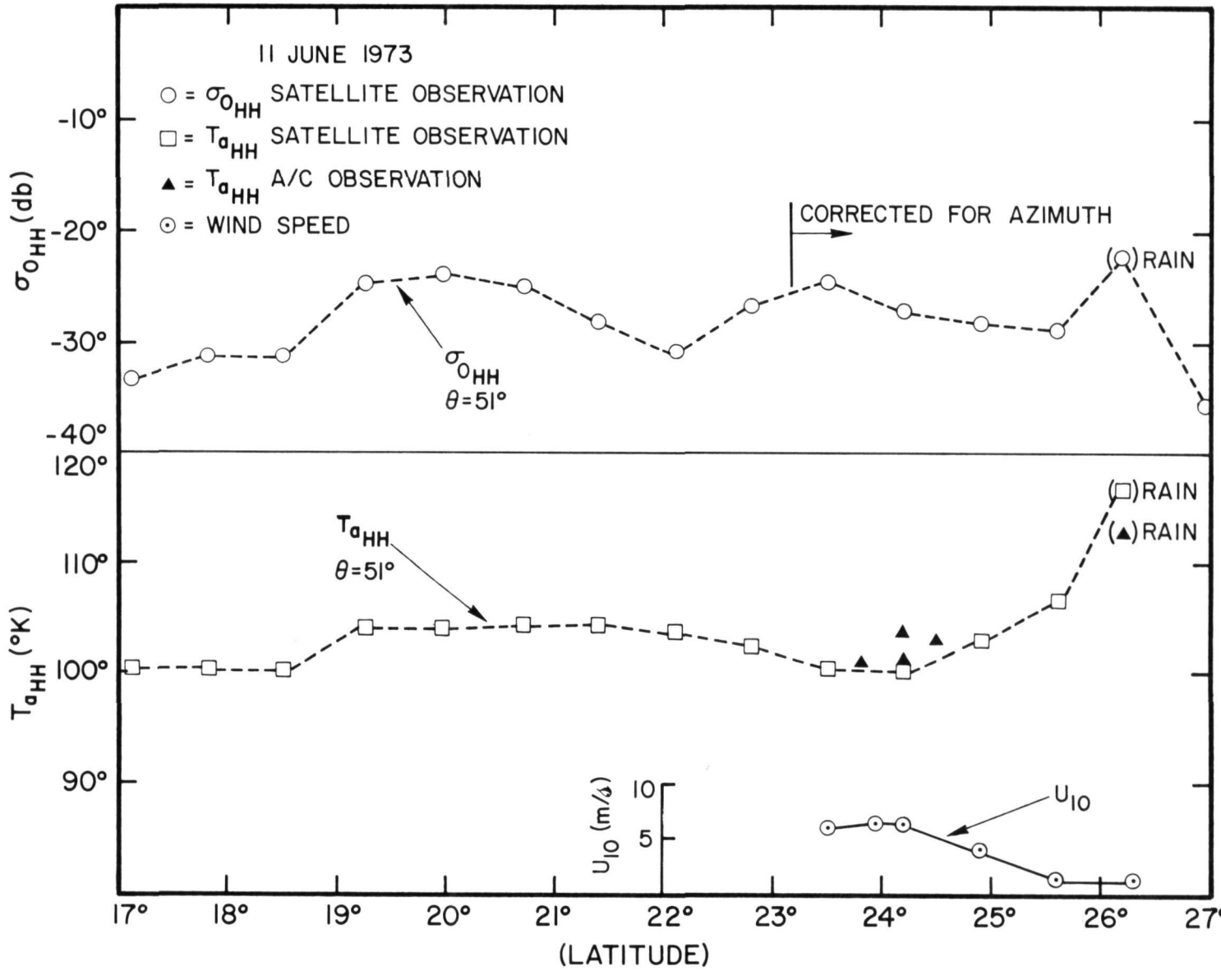

Figure 6. Skylab pass of 11 June in the Gulf of Mexico.

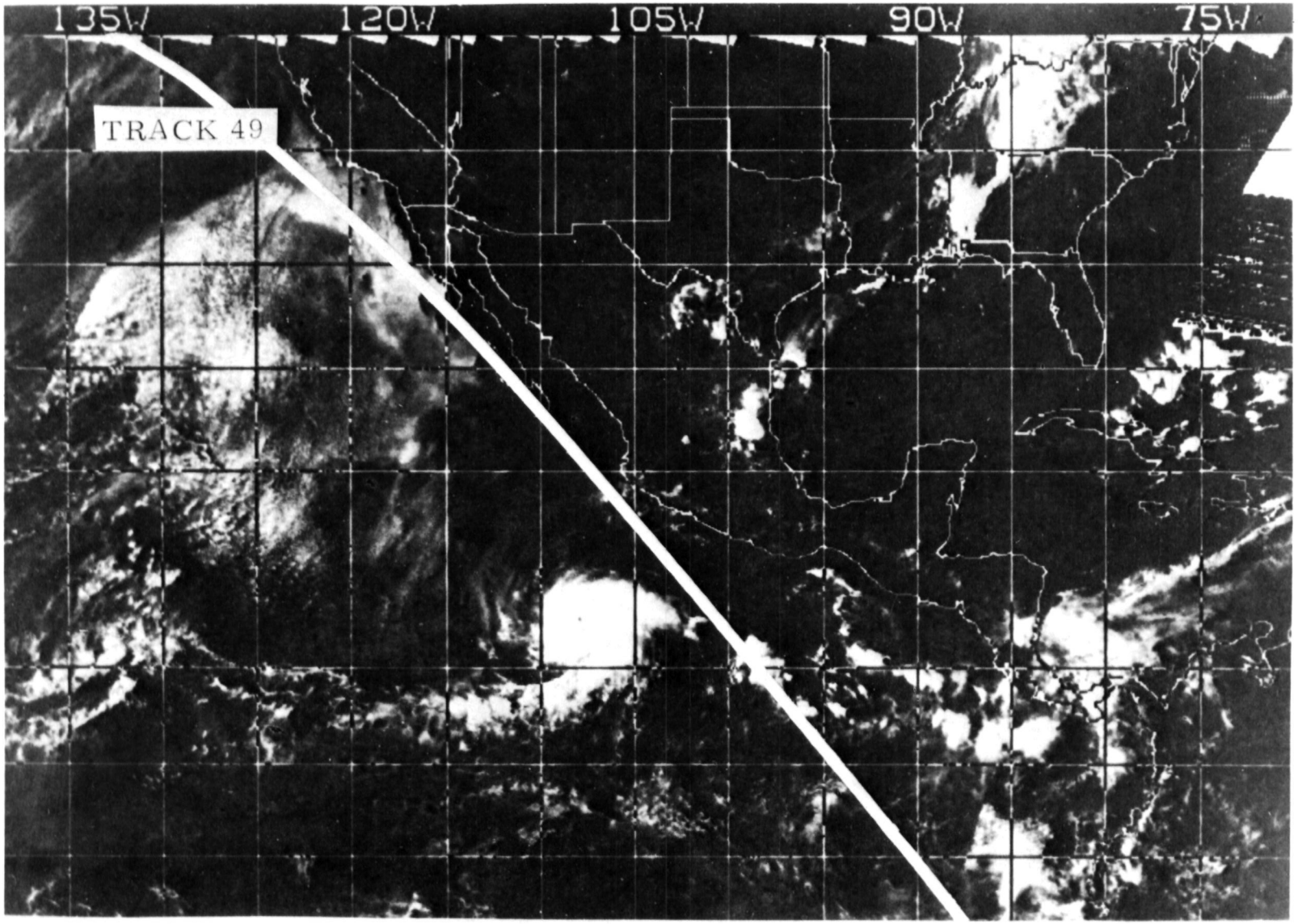

Figure 7. Hurricane Ava, June 6, 1973, NOAA-2 composite showing track of Skylab satellite.

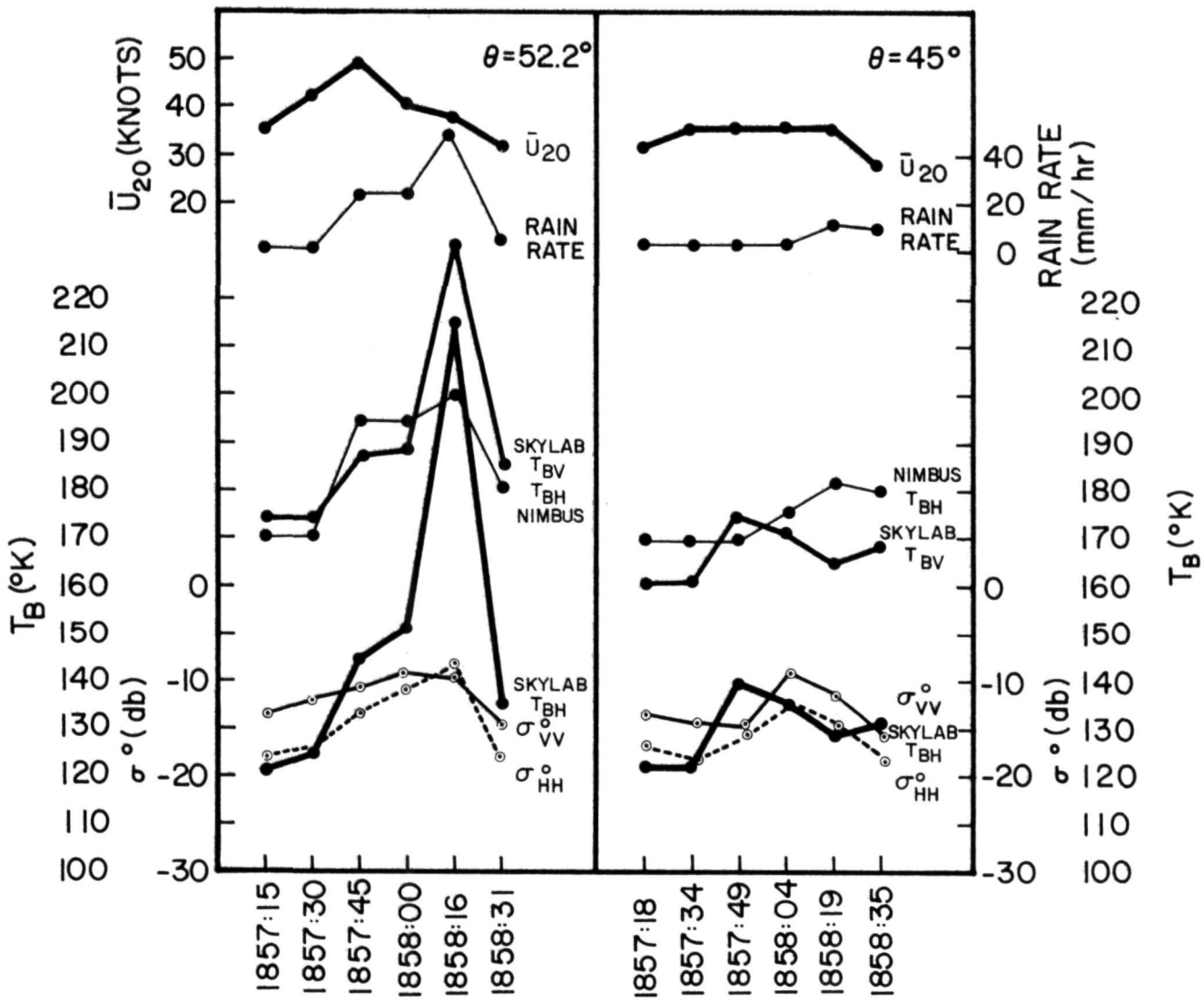

Figure 8. Skylab and NIMBUS-E data in Hurricane Ava.

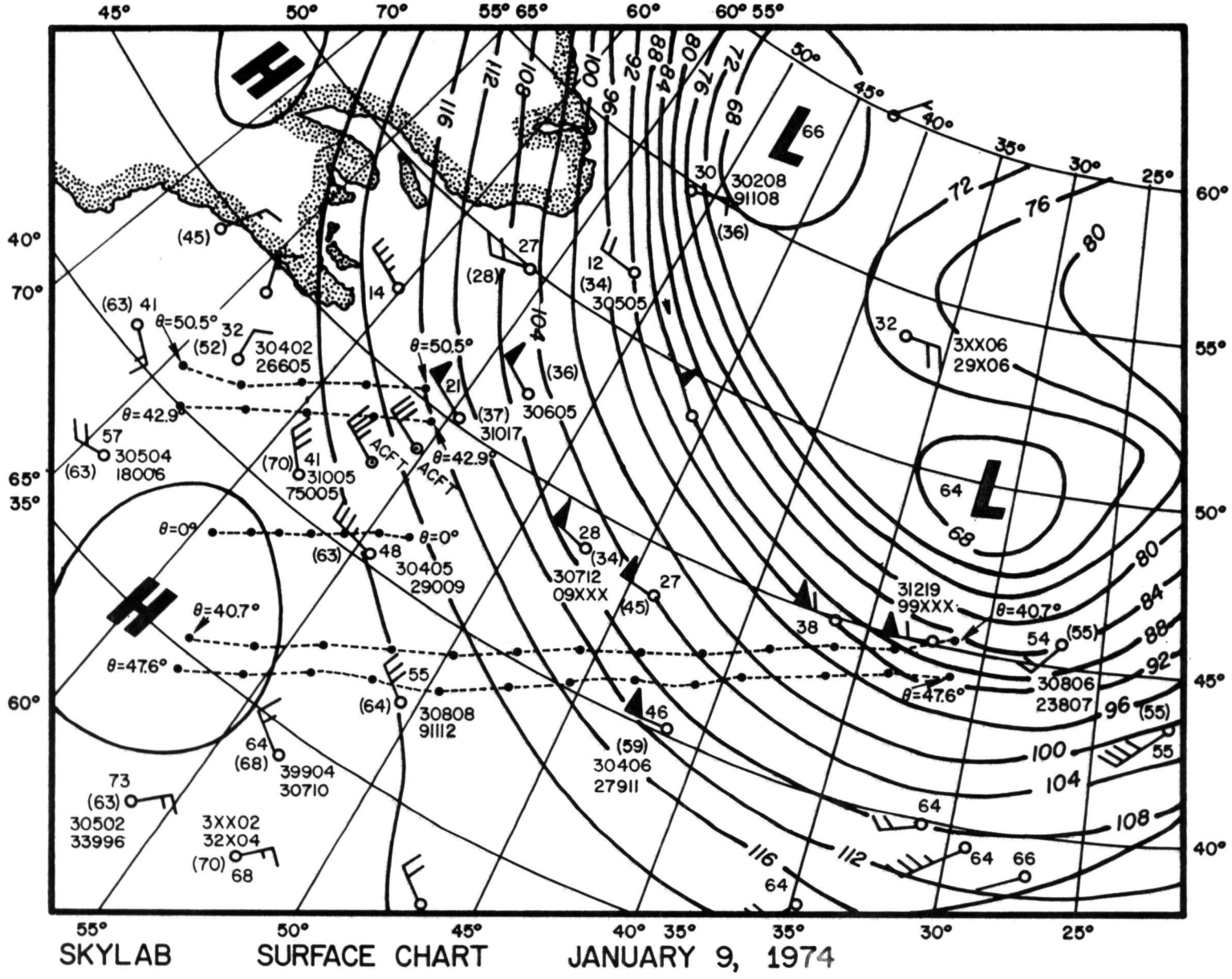

Figure 9. Surface meteorological analysis for 9 January 1974 pass. Subsatellite positions of S-193 under study are shown for the indicated incidence angles.

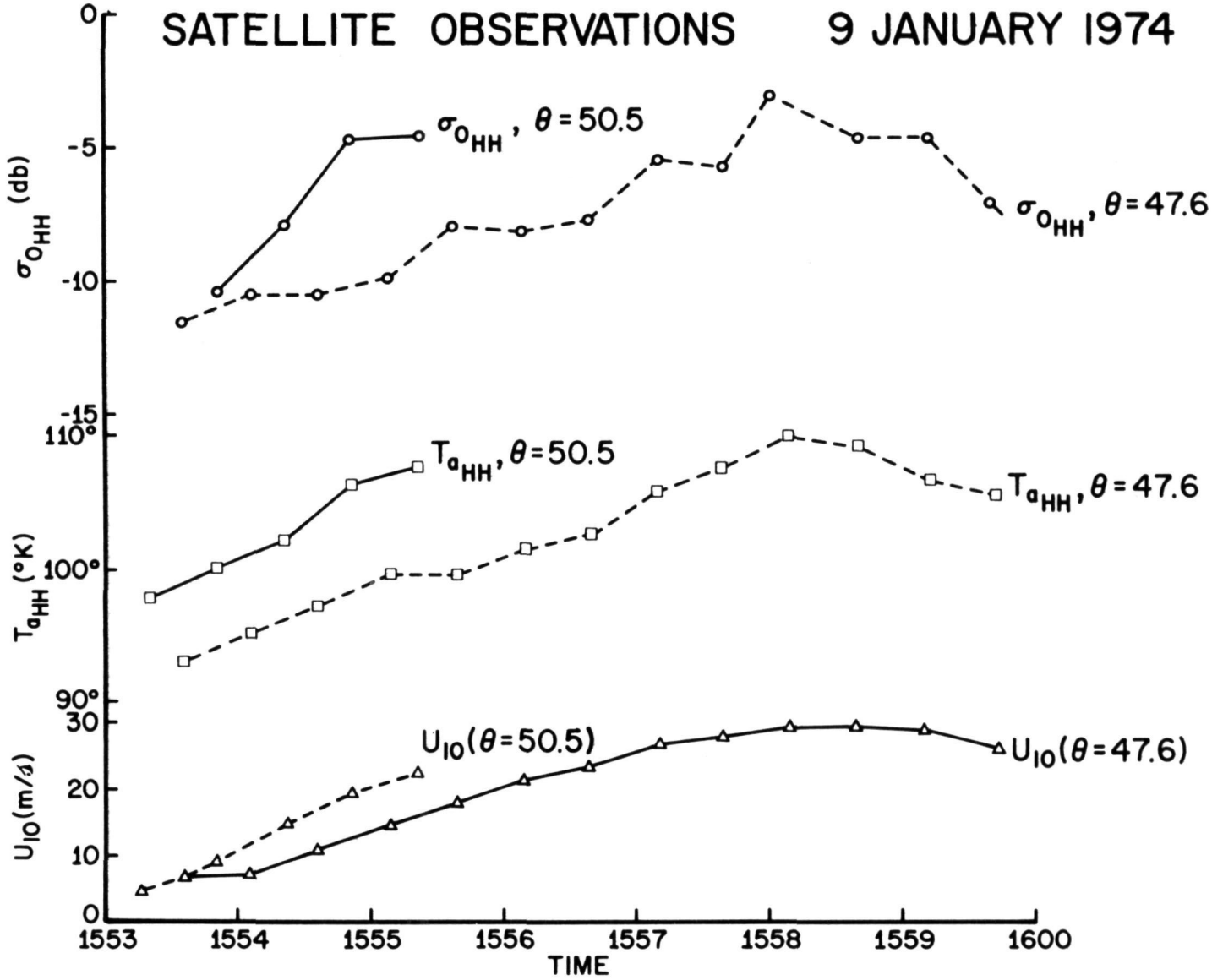

Figure 10. S-193 data during the 9 January pass along with surface winds determined from the surface analysis.

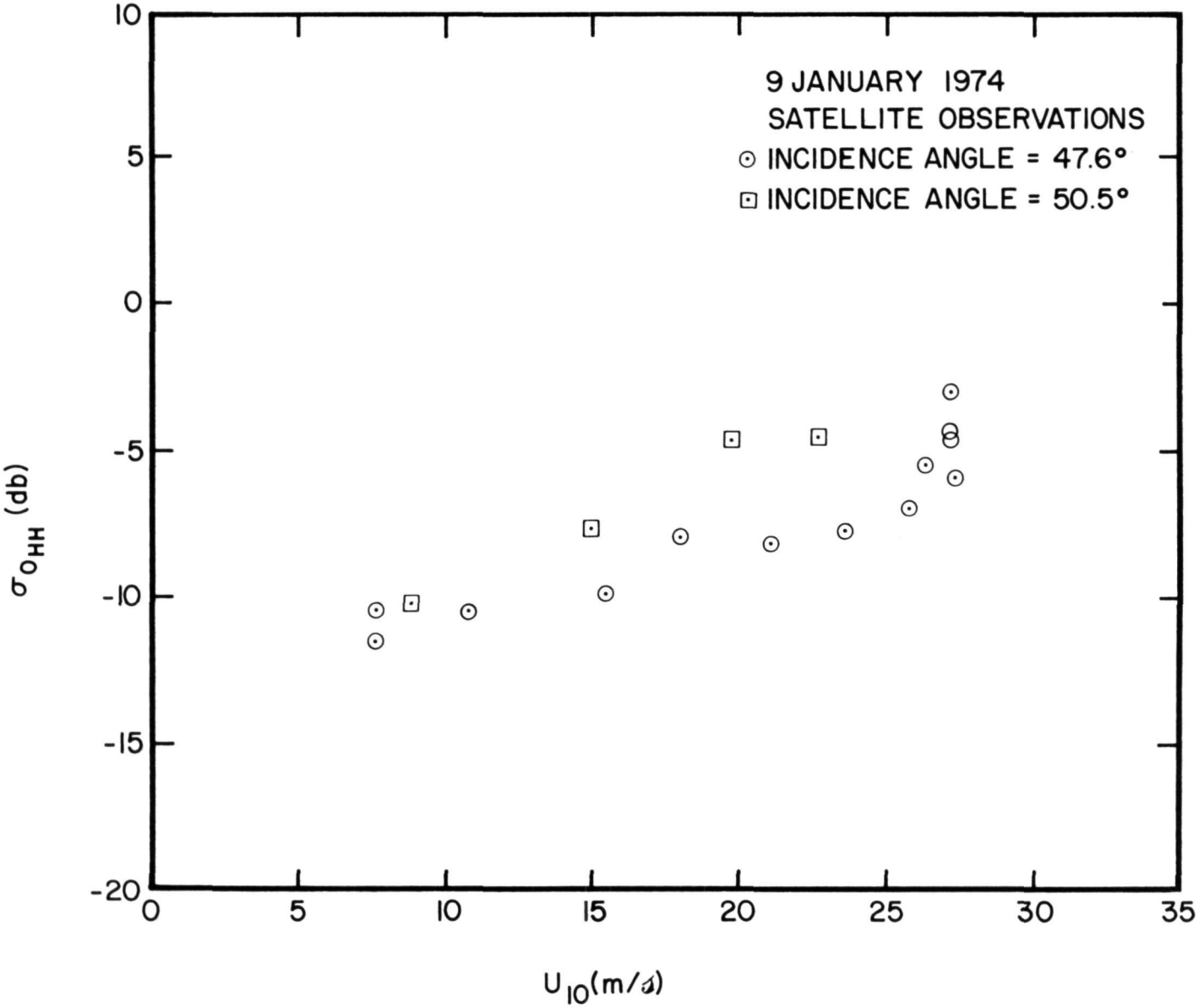

Figure 11. Radar backscatter, σ_0 versus windspeed for 9 January.

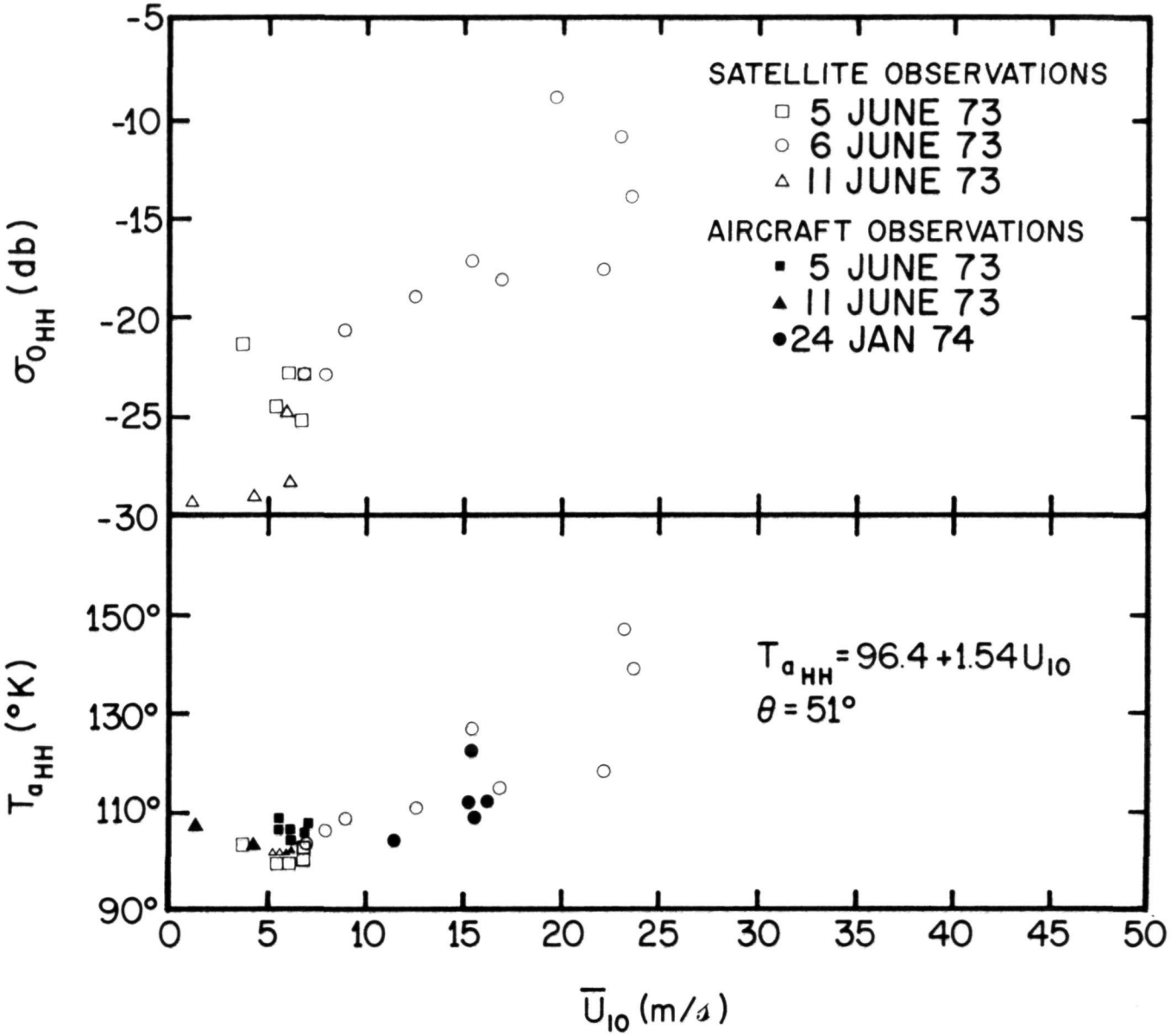

Figure 12. Radar backscatter and antenna temperature versus windspeed during SL-2.

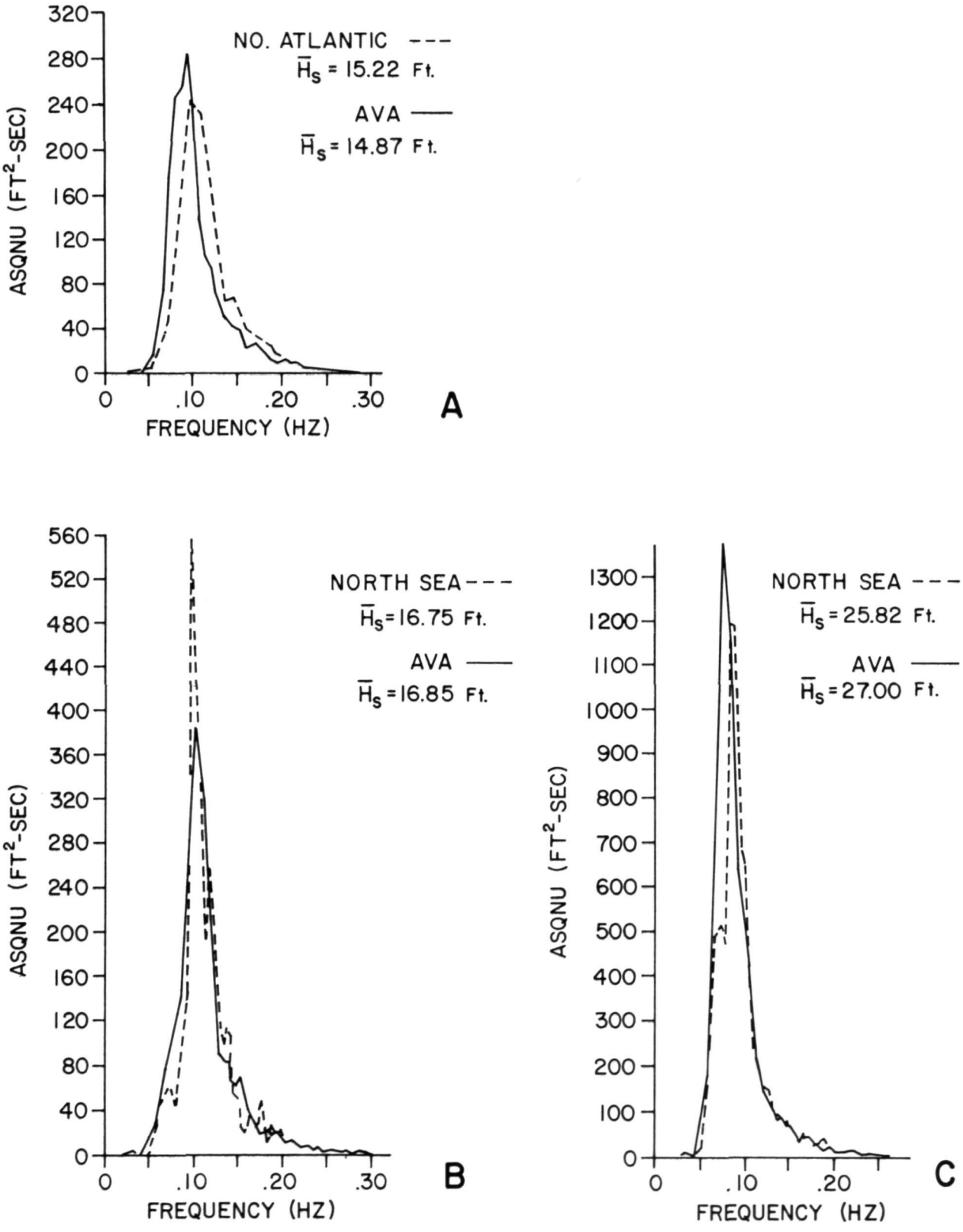

Figure 13. Wave spectra measured during the aircraft penetration of Hurricane Ava along with North Sea spectra for fetch-limited 25 m/sec winds.

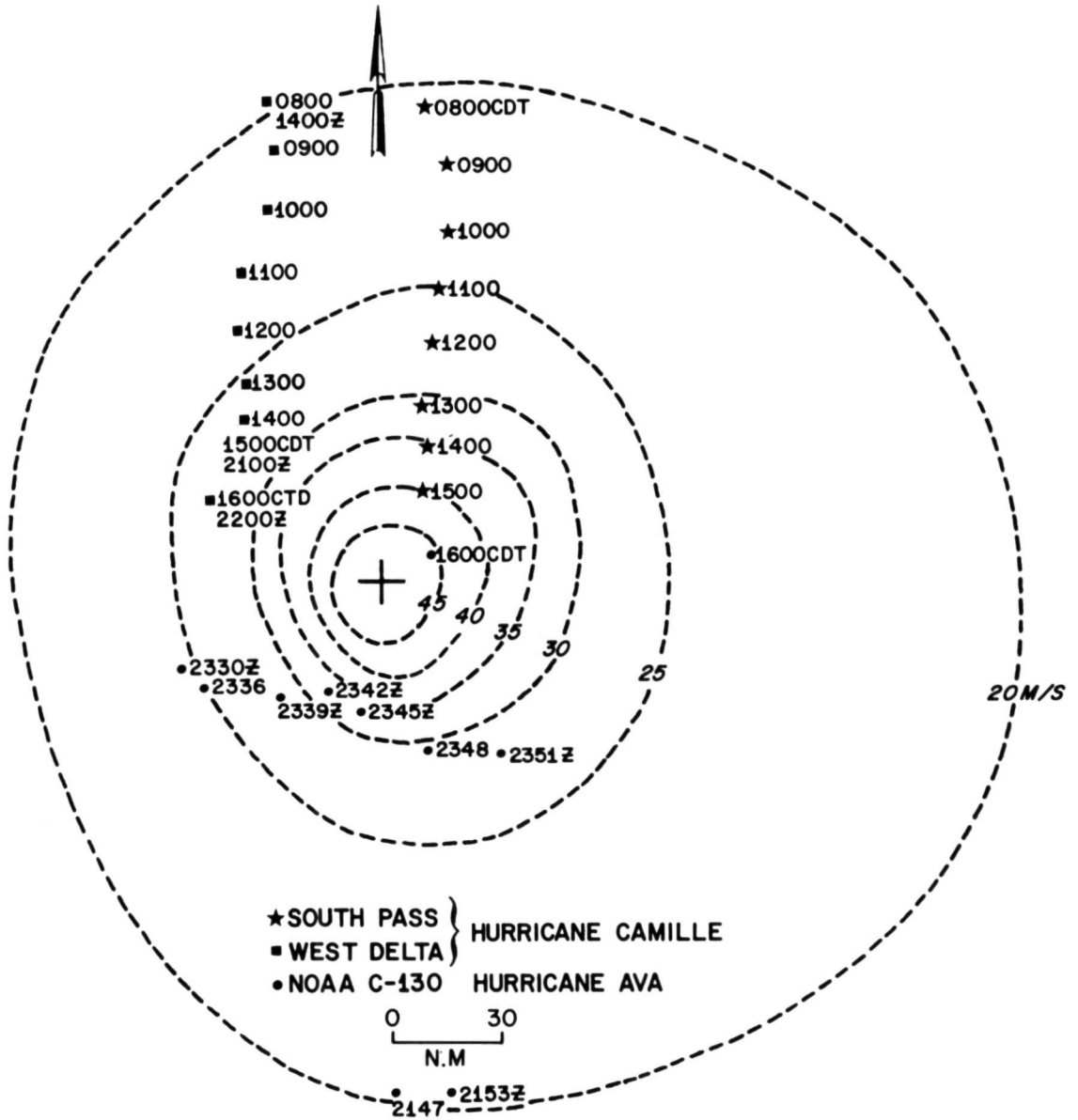

Figure 14. Surface wind analysis for hurricane Ava constructed from aircraft data along with relative positions of wave data obtained in Ava and for Hurricane Camille.

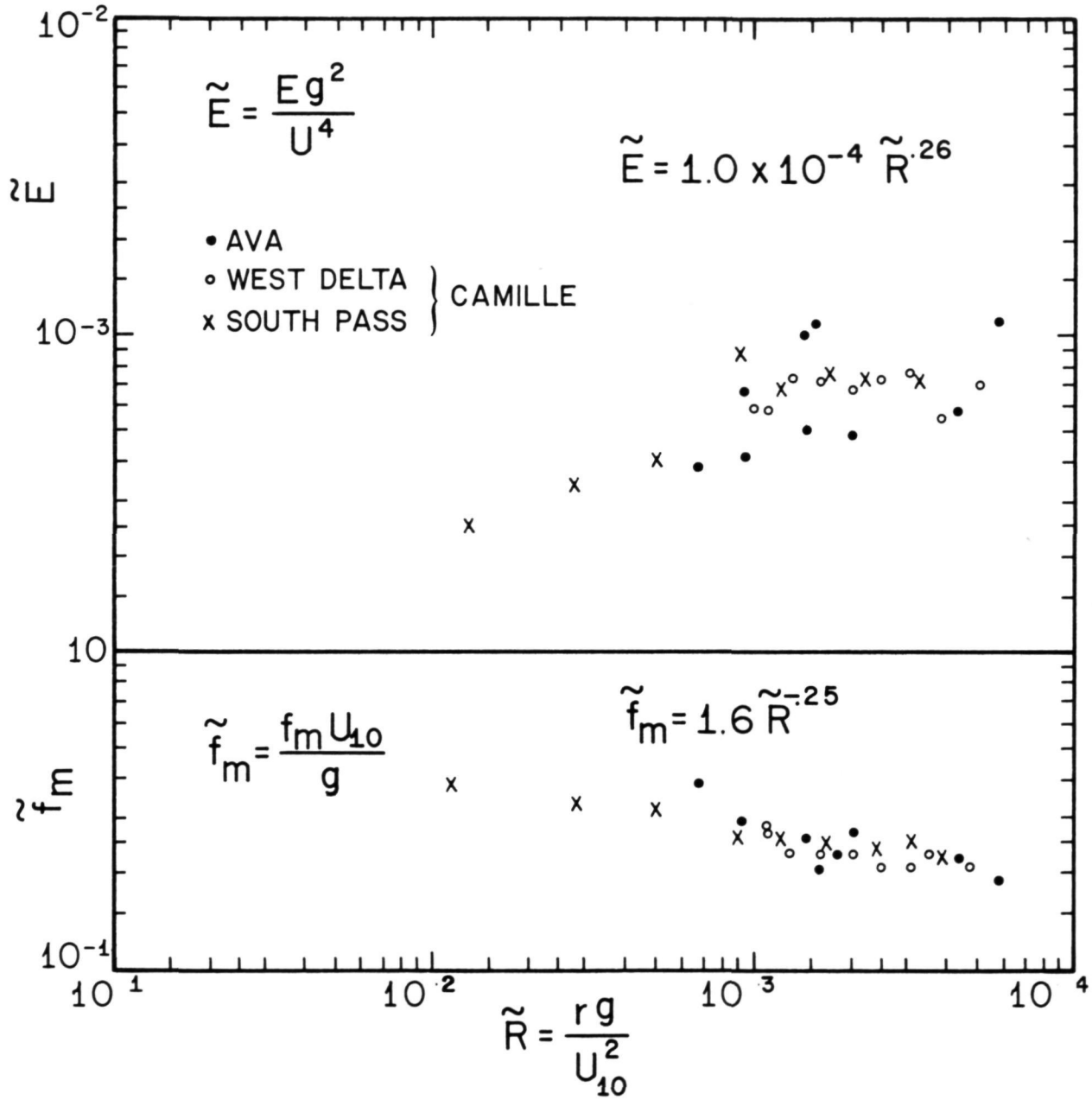

Figure 15. Behavior of nondimensional energy, E, and peak frequency, $\tilde{f}_m$, versus radial distance from eye. $\tilde{R} \approx 10^2$ constitutes the region of maximum winds.

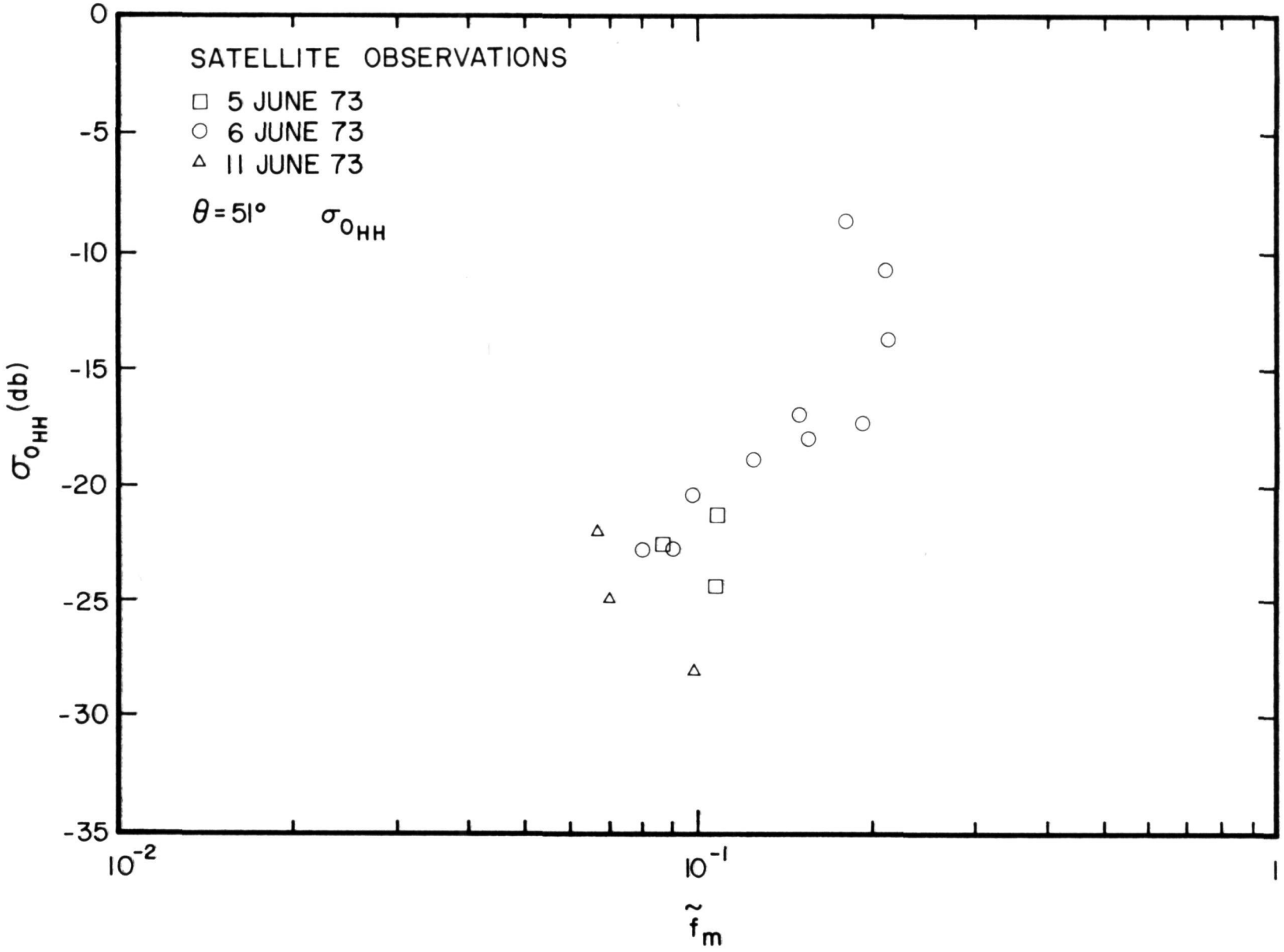

Figure 16. Radar backscatter, σ_0, versus stage of wave development as represented by non-dimensional peak frequency $\tilde{f}_m$ for the SL-2 data set.